

## IMMUNOGENOMICS

# Human fetal microglia acquire homeostatic immune-sensing properties early in development

L. Kracht<sup>1\*</sup>, M. Borggrewe<sup>1\*</sup>, S. Eskandar<sup>1,2\*</sup>, N. Brouwer<sup>1</sup>, S. M. Chuva de Sousa Lopes<sup>3,4</sup>, J. D. Laman<sup>1</sup>, S. A. Scherjon<sup>2</sup>, J. R. Prins<sup>2</sup>, S. M. Kooistra<sup>1†‡</sup>, B. J. L. Eggen<sup>1†‡</sup>

**M**icroglia, immune cells of the central nervous system (CNS), are important for tissue development and maintenance and are implicated in CNS disease, but we lack understanding of human fetal microglia development. Single-cell gene expression and bulk chromatin profiles of microglia at 9 to 18 gestational weeks (GWs) of human fetal development were generated. Microglia were heterogeneous at all studied GWs. Microglia start to mature during this developmental period and increasingly resemble adult microglia with CNS-surveilling properties. Chromatin accessibility increases during development with associated transcriptional networks reflective of adult microglia. Thus, during early fetal development, microglia progress toward a more mature, immune-sensing competent phenotype, and this might render the developing human CNS vulnerable to environmental perturbations during early pregnancy.

**M**icroglia are the resident myeloid cells of the central nervous system (CNS) and contribute to tissue homeostasis and pathology. Under homeostasis, microglia survey the CNS parenchyma and express receptors involved in monitoring and immune-sensing functions, termed the sensome (1). Microglia colonize the brain prior to neurogenesis, myelination, and blood-brain barrier formation and are a largely self-maintaining and long-lived population in healthy CNS (2, 3). Environmental perturbations during pregnancy affect microglia functioning (4, 5) and can be associated with epigenetic reprogramming (6, 7). Microglia are important for CNS development, and in view of their longevity and epigenetic memory, early perturbations in microglia might have long-lasting effects that could affect CNS development and function (8, 9).

In mice, microglia emerge from early erythromyeloid progenitors in the extraembryonic yolk sac at embryonic day 7.5 (E7.5) and subsequently colonize the developing brain rudiment at E9.5 (10). Mouse microglia development is accompanied by changes in gene expression and epigenetic profiles (5). Microglia proliferate and differentiate in early embryonic stages and support neuronal development (synaptic pruning) in late embryonic and early postnatal stages. They acquire their homeostatic and

immune surveillance profile at late postnatal and adult stages (4, 5). During embryonic development and early postnatal stages, mouse microglia are heterogeneous (11–13).

In human embryos, shortly after the closure of the neural tube, amoeboid ionized calcium-binding adaptor protein 1-positive (IBA1<sup>pos</sup>) microglia appear at gestational week (GW) 4.5 in the leptomeninges, the ventricular edge, and the choroid plexus of the brain (14). From these sites, microglia colonize the telencephalon and diencephalon. During this process, microglia transform to ramified cells, which are recognizable as early as GW12 (15, 16).

To date, limited bulk RNA sequencing (RNA-seq) data of human mid-gestation fetal microglia indicate that mouse and human microglia share developmental gene expression signatures (4). However, an in-depth understanding of cellular development and heterogeneity of microglia during human fetal development is lacking. Here, 15,782 microglia were analyzed with single-cell RNA sequencing (scRNA-seq), and underlying gene regulatory mechanisms were observed by assay for transposase-accessible chromatin sequencing (ATAC-seq) in 23 human fetuses ranging from GW9 to -18.

## Isolation and characterization of microglia from human fetal CNS tissue

Single-cell transcriptional profiles ( $n = 20$  fetuses) and chromatin accessibility ( $n = 8$  fetuses) were generated from viable [4',6-diamidino-2-phenylindole-negative, DRAQ5<sup>positive</sup> (DAPI<sup>neg</sup>DRAQ5<sup>pos</sup>)] human fetal microglia (CD11B<sup>pos</sup>CD45<sup>int</sup>) that were isolated by fluorescence-activated cell sorting (FACS) of CNS tissue from 23 early to mid-gestation (GW9 to -18) fetuses after elective pregnancy termination (Fig. 1, A and B, and table S1). Using a modified Smart-seq2 scRNA-seq protocol, we sequenced 15,782 microglia and 781 nonmicroglia CNS cells, with a median number

of 22,330 unique molecular identifiers (UMIs) and 977 unique genes per cell after filtering. The number of UMIs and percentages of ribosomal and mitochondrial RNA were similar across all samples and ages (fig. S1, A and B). To verify that the CD11B<sup>pos</sup>CD45<sup>int</sup> population was microglia, we compared the transcription profile to CNS cell type-specific gene sets from two independent human datasets (17, 18) (table S2). Expression of microglia genes was enriched in CD11B<sup>pos</sup>CD45<sup>int</sup> microglia, but not in other (CD11B<sup>neg</sup>CD45<sup>neg</sup>) CNS cells (Fig. 1C). IBA1 immunoreactivity was detected in fetal CNS tissue at all gestational ages, and a typical ramified microglia morphology was observed in most tissues, confirming the presence of microglia (Fig. 1D).

## Microglia are heterogeneous during human fetal development and exhibit an activated, phagocytic gene expression profile

To determine transcriptional microglia heterogeneity during development, we performed an unsupervised clustering analysis, resulting in 16 distinct clusters (Fig. 2A) present at all GWs (Fig. 2B). All clusters exhibited similar amounts of mitochondrial and ribosomal RNA and UMIs per cell (fig. S1C). Thus, cluster formation was not caused by differences in cell quality. Variation between samples was minor, and sample bias did not affect clustering (fig. S2A). Although sex did not affect cluster distribution (fig. S2B), male/female gene expression differences were difficult to assess, owing to unequal male and female sample numbers per GW (table S1). Clusters were annotated on the basis of cluster-enriched genes (fig. S2, C and D, and table S3), which were determined by differential gene expression analysis of one cluster compared with all other clusters.

Cells in myeloid clusters 9 and 10 expressed the nonmicroglia myeloid cell markers *LYVE1* and *S100A9*, respectively (fig. S2, C and D). These clusters also expressed genes of the *MS4A* family, which have been associated with a microglia-brain border macrophage intermediate during mouse development (13). Microglia clusters 11 to 16 were characterized on the basis of unique expression of cluster-enriched genes *MRPL23*, *PARP4*, *MTXI*, *HBA/HBG*, *ZP3*, and *NAMPT* (fig. S2, C and D).

All microglia clusters expressed canonical microglia markers *CSF1R* and *CX3CR1* (Fig. 2C). Expression of homeostatic microglia genes *P2RY12* (Fig. 2C), *P2RY13*, and *TMEM119* (fig. S3A) was less frequent but present and validated in situ for TMEM119 (fig. S3, B and C). Microglia of all clusters expressed multiple genes previously associated with an activated, phagocytic microglia phenotype identified in aging and neurodegenerative diseases [also called the DAMs/MGnD (disease-associated microglia and microglial neurodegenerative) phenotype] (19–21) (Fig. 2C and fig. S3A). *AXL*, *APOE*, and *CD68*, markers for activated,

<sup>1</sup>Department of Biomedical Sciences of Cells and Systems, Section Molecular Neurobiology, University Medical Center Groningen, University of Groningen, Groningen, Netherlands.

<sup>2</sup>Department of Obstetrics and Gynecology, University Medical Center Groningen, University of Groningen, Groningen, Netherlands.

<sup>3</sup>Department of Anatomy and Embryology, Leiden University Medical Center, Leiden, Netherlands.

<sup>4</sup>Department for Reproductive Medicine, Ghent University Hospital, Ghent, Belgium.

\*These authors contributed equally to this work.

†These authors contributed equally to this work.

‡Corresponding author. Email: s.m.kooistra@umcg.nl (S.M.K.); b.j.l.leggen@umcg.nl (B.J.L.E.)

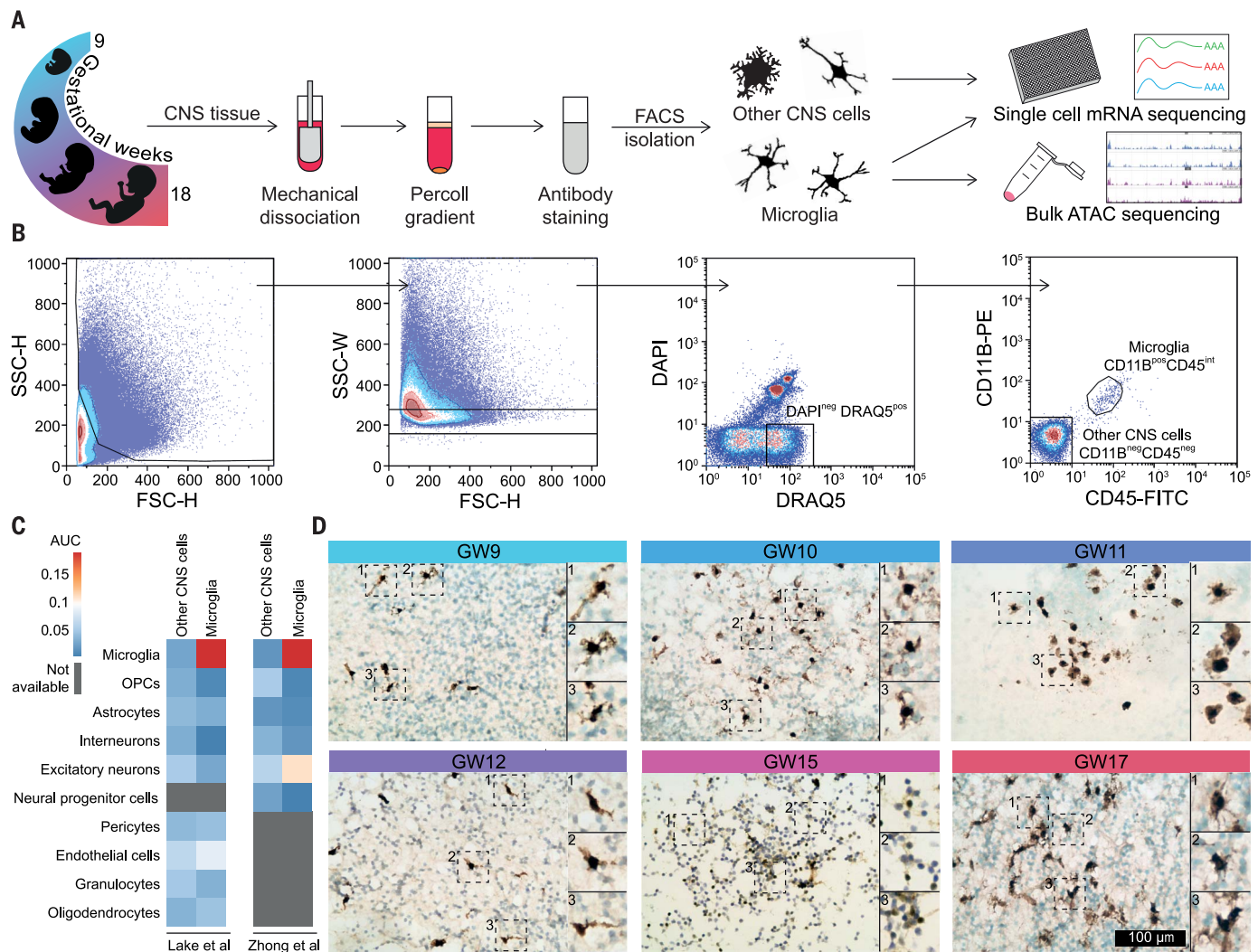


**Fig. 1. Study design and isolation of microglia from fetal CNS tissue.**

(A) CNS tissue from fetuses at GW9 to -18 was processed on ice with mechanical dissociation and Percoll gradient centrifugation (for GWs >12). Individual microglia and other CNS cells were sorted into 384-well plates for scRNA-seq ( $n = 20$ ). Bulk microglia were collected for ATAC-seq ( $n = 8$ ). (B) Representative FACS plots of the gating strategy for isolation of microglia and other CNS cells

( $n = 23$ ). FSC-H, forward scatter height; SSC-W, side scatter width; PE, phycoerythrin; FITC, fluorescein isothiocyanate. (C) Heatmap depicting expression of CNS cell type-specific gene sets from two different datasets (17, 18) (table S2) in FACS-isolated microglia and other CNS cells, reported as AUC values. (D) IBA1 immunoreactivity in CNS tissue of GW9 to -17 fetuses. Insets depict 2 $\times$  magnifications of the indicated areas. OPC, oligodendrocyte progenitor cell.

phagocytic microglia, colocalized with IBA1 in situ, confirming their expression by microglia (Fig. 2, D and E, and fig. S3D).

#### Microglia clusters are associated with GW and exhibit distinct functional profiles

In view of the GW-dependent distribution of cells on the uniform manifold approximation and projection (UMAP) (Fig. 3A) and the differential contribution to clusters (Fig. 2B), we characterized GW-associated clusters.

The percentage of cells in cluster 5 increased from GW9 to -18 and showed distinct expression of immediate-early genes (IEGs) (Fig. 3B). cJUN protein was also detected in IBA1<sup>pos</sup> microglia in situ (Fig. 3C), making artificial induction of IEGs exclusively by the microglia isolation procedure unlikely. Gene ontology

(GO) terms associated with the cluster-enriched genes were mainly immune- and inflammation-related (Fig. 3D and table S4).

Microglia from all gestational ages contributed to cluster 6, but it was enriched for cells from GW10 to -13 (Fig. 3E). Cells of cluster 6 uniquely expressed the cell cycle genes *MKI67* and *SPC24* (Fig. 3E), were annotated to G<sub>2</sub>/M and S phase on the basis of conserved cell cycle genes (fig. S2B), and were associated with GO term cell division (Fig. 3D and table S4). Immunostaining confirmed expression of *MKI67* in IBA1<sup>pos</sup> microglia across multiple GWs (Fig. 3F), indicating the presence of proliferating microglia.

Clusters 7 and 8 had a strong bias for GW9 to -10 microglia, whereas these clusters had little contribution of cells from GWs >15 (Fig. 3G).

Cluster-enriched genes included neuronal genes and phagocytosis genes (Fig. 3G and H). Phagocytosis of other cells or debris may explain the presence of these neuronal transcripts.

More than 40% of microglia in clusters 2 and 3 were derived from GW11 to -12 samples (Fig. 3H). Although microglia of all clusters expressed genes associated with microglia activation (Fig. 2, C, D, and E), some of these genes were more enriched in GW11 to -12 microglia (Fig. 3H). GO terms associated with GW11 to -12 microglia cluster-enriched genes were related to phagocytosis and brain development (Fig. 3D and table S4).

Clusters 1 and 4 exhibited higher expression of homeostatic microglia markers and primarily contained cells from GW15 to -17 (Fig. 3I). Homeostatic markers CX3CR1 and VISTA

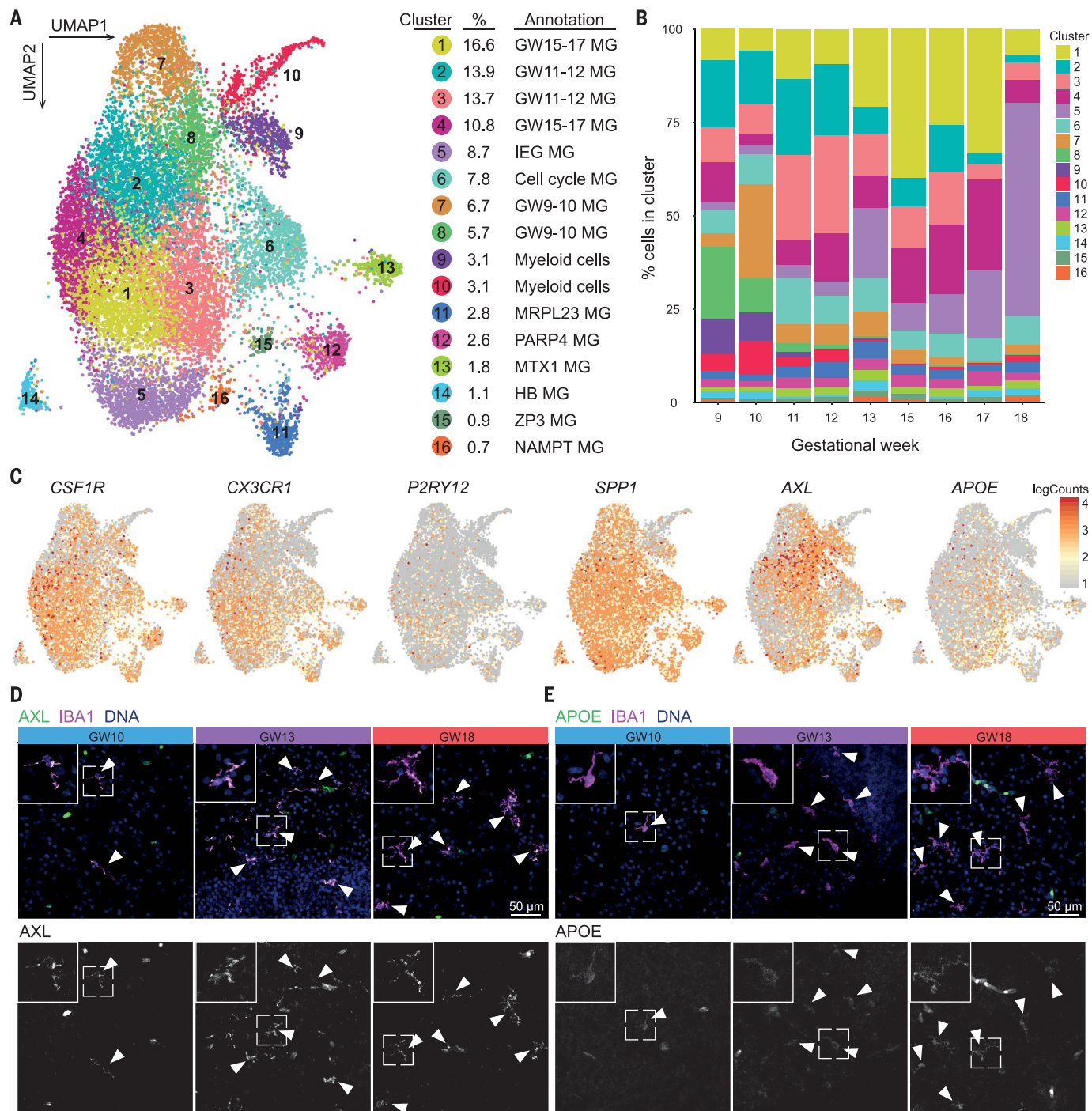


**Fig. 2. Human fetal microglia are heterogeneous and exhibit an activated, phagocytic profile.** (A) UMAP of 15,782 cells and 16 clusters depicted with size (percentage of total cells in a specific cluster) and annotation (20 fetal samples;  $n = 1$  to 4 per GW). (B) Bar plots depicting the percentage of cells in each cluster

at different GWs. (C) UMAPs depicting expression of microglia markers in log counts. (D and E) AXL and IBA1 (D) and APOE and IBA1 (E) coexpression in CNS tissue of GW10 to -18 fetuses. Lower images show single channels. White arrowheads indicate colocalization. Insets depict 2 $\times$  magnifications of the indicated areas. MG, microglia.

colocalized with IBA1 in situ (fig. S3, E and F), demonstrating their expression by microglia (22). Enriched genes of GW15 to -17 microglia were annotated with GO terms for cytokine and immune system processes (Fig. 3D and table S4).

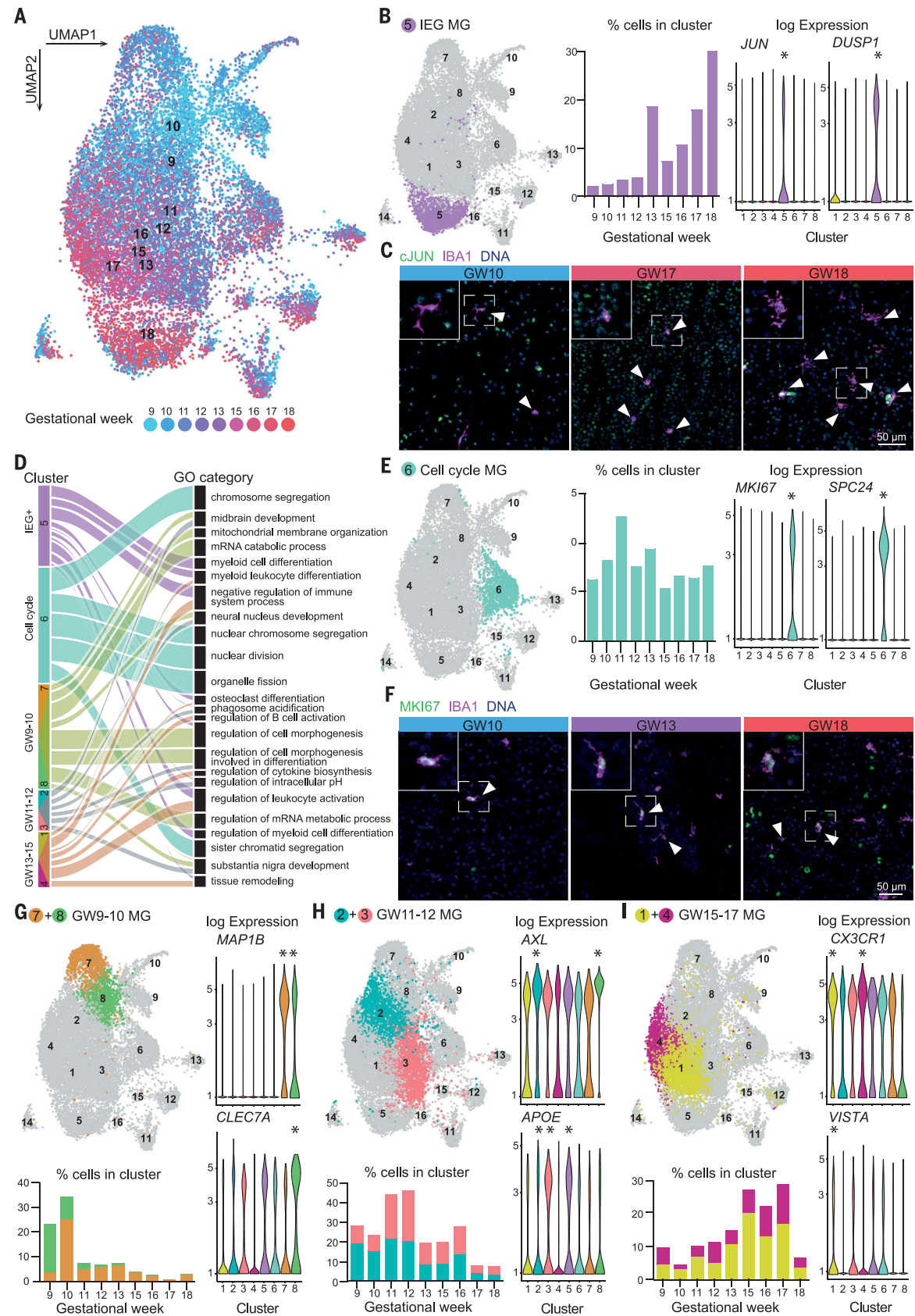
#### Microglia undergo developmental transition toward adult, homeostatic microglia

To further delineate the observed developmental progression (Fig. 3), we performed pseudotime analysis (23). Assigned pseudotimes (Fig. 4A) corresponded with the gestational ages

(Fig. 4B), suggesting a GW-dependent trajectory. This trajectory contained seven segments, or states, which were separated by branching points (Fig. 4, A and C), and differential gene expression analysis was performed to identify state-enriched genes (table S5). State

**Fig. 3. GW-associated microglia clusters have diverse functional profiles.**

(A) UMAP depicting GWs (20 fetal samples;  $n = 1$  to 4 per GW). (B) UMAP highlighting specific cluster, bar plots indicating the percentage of cells in cluster across GWs, and violin plots depicting log expression of cluster-enriched genes for IEG MG. (C) cJUN and IBA1 coexpression in CNS tissue of GW10 to -18 fetuses. (D) Alluvial plot depicting the top five GO terms per cluster, plotted for all clusters. Ribbon thickness reflects the number of genes in GO terms. (E) UMAP highlighting specific cluster, bar plots indicating the percentage of cells in cluster across GWs, and violin plots depicting log expression of cluster-enriched genes for cell cycle MG. (F) MKI67 and IBA1 (F) coexpression in CNS tissue of GW10 to -18 fetuses. (G to I) UMAPs highlighting specific clusters, bar plots indicating the percentage of cells in respective clusters across GWs, and violin plots depicting log expression of cluster-enriched genes for GW9 to -10 MG (G), GW11 to -12 MG (H), and GW15 to -17 MG (I). Significantly enriched genes per cluster, compared with all other clusters, are indicated. \* $P$ (adjusted) < 0.05, model-based analysis of single-cell transcriptomics (MAST). White arrowheads indicate colocalization. Insets depict 2 $\times$  magnifications of the indicated areas. MG, microglia.



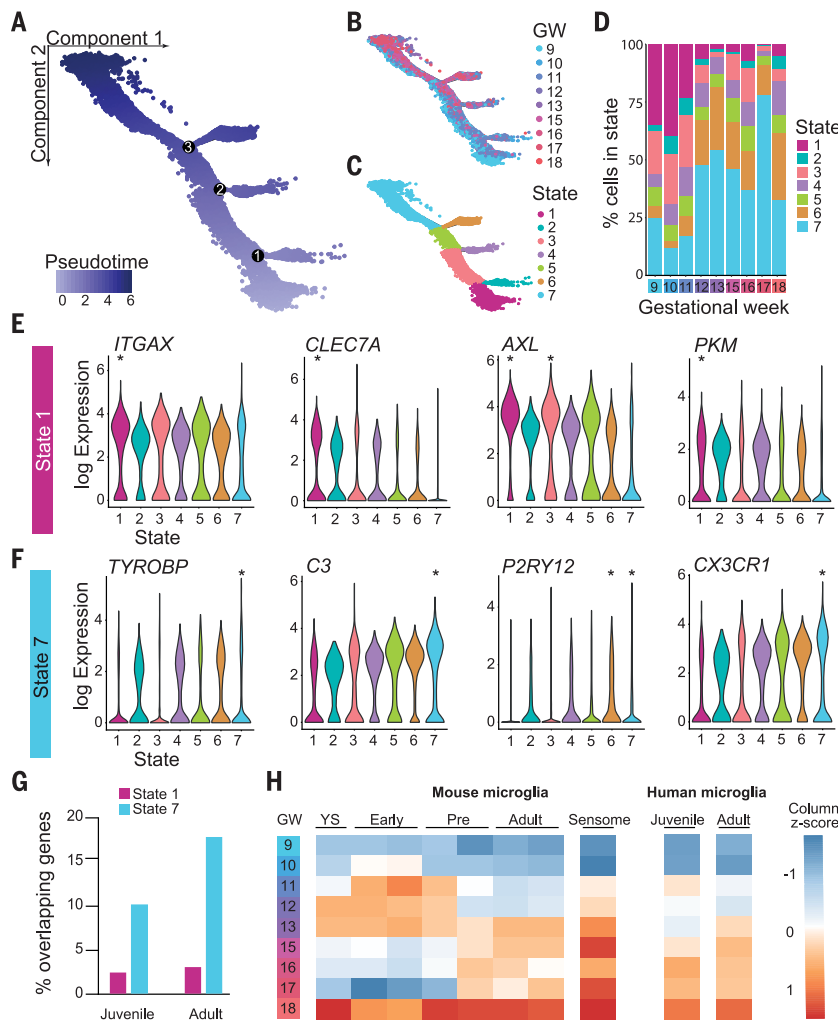


**Fig. 4. Developmental progression toward homeostatic microglia.** (A to C) Trajectory plots depicting pseudotime (numbers indicate branching points) (A), GW (B), and state (C). (D) Bar plots depicting the percentage of microglia in each state at different GWs. (E and F) Violin plots of log expression of state-enriched genes for state 1 (GW9 to -11) (E) and state 7 (GW12 to -18) (F). Significantly enriched genes per state were compared to all other states. \*P(adjusted) < 0.05, MAST test. (G) Bar plot depicting the percentages of overlapping genes between state 1 and 7 genes (table S6) with the top 500 human juvenile (26) and adult (27) microglia genes (table S2). (H) Heatmap depicting enrichment of mouse developmental stage genes (5), mouse sensome (1), and human juvenile (26) and adult microglia (27) genes (table S2) across GWs visualized as column z-scores of AUC values. YS, yolk sac.

formation was not driven by individual samples (fig. S4A).

State-enriched genes of side branches (states 2, 4, and 6) were associated with oxidative phosphorylation, cell cycle, and the immediate-early response (table S5). Whether these side branches represent distinct cell fates or transient transcriptional divergences from the main trajectory is not clear.

State 1 contained mainly GW9 to -11 microglia, whereas state 7 largely consisted of GW12 to -18 microglia (Fig. 4D), which is consistent with the GW-associated clusters (fig. S4B). State 1-enriched genes were associated with microglia development (24), microglia

activation and phagocytosis (19, 20), and glycolysis (13, 25) (Fig. 4E and fig. S4C). Over the pseudotime trajectory, expression of homeostatic sensome markers and a different set of microglia activation markers increased, and this was most pronounced in state 7 (Fig. 4F and fig. S4D).

To confirm the developmental progression of fetal microglia, we compared their transcriptional profiles with profiles of mouse developmental microglia (5), the mouse sensome (1), and juvenile (26) and adult human microglia (27) (Fig. 4, G and H, and table S2). The overlap with juvenile and adult microglia genes increased from ≈2 to 3% of state 1 genes

to 10 to 18% of state 7 genes (Fig. 4G), suggesting developmental progression of human microglia from GW9 to -11 (state 1) to GW12 to -18 (state 7). Progressive enrichment of mouse and human microglia gene sets in GW9 to -18 fetal microglia was determined using area under the curve (AUC) analysis (Fig. 4H). Microglia younger than GW13 were enriched for genes from yolk sac and early mouse microglia (E10 to -16.5), and microglia older than GW13 were enriched for genes from pre- and adult microglia (P3 to -56), with the exception of GW18 microglia, which were enriched for genes at all developmental stages (Fig. 4H). An increasing overlap with mouse sensome genes was observed with progressing fetal GW (Fig. 4H). Also, enrichment of human juvenile and adult microglia genes gradually increased in fetal microglia with increasing GW (Fig. 4H). Together, these data suggest that microglia progress toward a homeostatic state during early human fetal development.

#### Distinct gene regulatory networks are active in early and mid-gestational microglia

Mouse microglia development is orchestrated by distinct transcription factors (TFs) (5). To unravel putative gene regulatory mechanisms underlying the transcriptional changes in developing human fetal microglia, single-cell regulatory network inference and clustering (SCENIC) (28) was used. SCENIC analyzes co-expression and TF motifs in scRNA-seq data.

Sixty-six gene regulatory networks were identified that segregated into two main hubs after unsupervised clustering associated with older and younger GWs (Fig. 5A). Gene regulatory networks associated with younger GWs were enriched for diverse general cellular functions, including cell cycle (E2F2), morphogenesis (SOX4/11), and differentiation and chromatin remodeling (SP1) (29) (Fig. 5, A and B). Gene regulatory networks associated with older GWs were more microglia specific, including many ETS TF family members, such as ETS1-2, ELF1, ELK3, and SPI1 (PU.1) (Fig. 5, A and C), which are crucial for microglia development and function (30, 31). Furthermore, gene regulatory networks associated with IEGs were identified in older GWs (Fig. 5A), and JUN activity overlapped with the IEG microglia cluster (Fig. 5C). These data show that gene regulatory networks progress from more general cellular functions in young GWs to microglia-specific properties in older GWs.

To verify scRNA-seq data-derived differences in gene regulatory network activity between microglia from young and old GWs, we assessed chromatin accessibility with ATAC-seq (Fig. 5, D and E, and fig. S5). The DNA sequences underlying peaks were analyzed for enrichment of putative TF-binding motifs

with HOMER (32). In the combined peaks of all samples, putative binding motifs of essential microglia TFs were enriched (table S7). Differential peak analysis indicated that more peaks were associated with older (GW >13; 1338 peaks) than with younger developmental stages (GW <13; 33 peaks) (Fig. 5D and table S8). In peaks that were enriched in microglia at GW <13, the SP1 TF motif was present, which was also detected by SCENIC (Fig. 5, A, B, and E). DNA sequences underlying peaks enriched in microglia at GW >13 contained many ETS TF family motifs, including PU.1 (Fig. 5E), which was validated at the protein level (Fig. 5F), in agreement with the SCENIC results (Fig. 5, A and C). These findings indicate that increased chromatin accessibility during microglia development is accompanied by the activation of gene networks driving microglia-specific functions.

## Discussion

Microglia are the CNS-resident myeloid cells and are critical for brain development and later tissue homeostasis (4, 5). After seeding the developing CNS from the yolk sac, and also closure of the blood-brain barrier, microglia form a self-sustained population with highly variable turnover and with negligible contribution from peripheral immune cells (33). Studies in mice have revealed that during development, different gene regulatory networks drive microglia proliferation, differentiation, and maturation and that perturbances have long-lasting functional consequences (4, 5).

Here, the transcriptomic profile and chromatin organization of human fetal microglia during early to mid-gestation (GW9 to -18) development are presented. In contrast to microglia in the healthy adult CNS (34), we found that fetal microglia are highly heterogeneous. They progressively mature from GW13 onward, which is regulated by the activity of increasingly complex gene regulatory networks, and they already display functional properties characteristic of mature human microglia at mid-gestation.

Human fetal microglia share extensive transcriptional similarities with microglia during mouse development, with analogous proliferative, glycolytic, and activated, phagocytic capacities (4, 12, 13). The presence of glycolysis-related genes in microglia at GW9 to -10 underscores their undifferentiated and activated state, since immune-activated mouse and human microglia (25, 35) as well as undifferentiated cells such as stem cells (36) and embryonic cells (13) use glycolysis as an energy source.

Early to mid-gestation microglia share transcriptional features with a phagocytic microglia population that is transiently present during postnatal mouse development and associated with myelinating brain regions (12, 13). In mice,

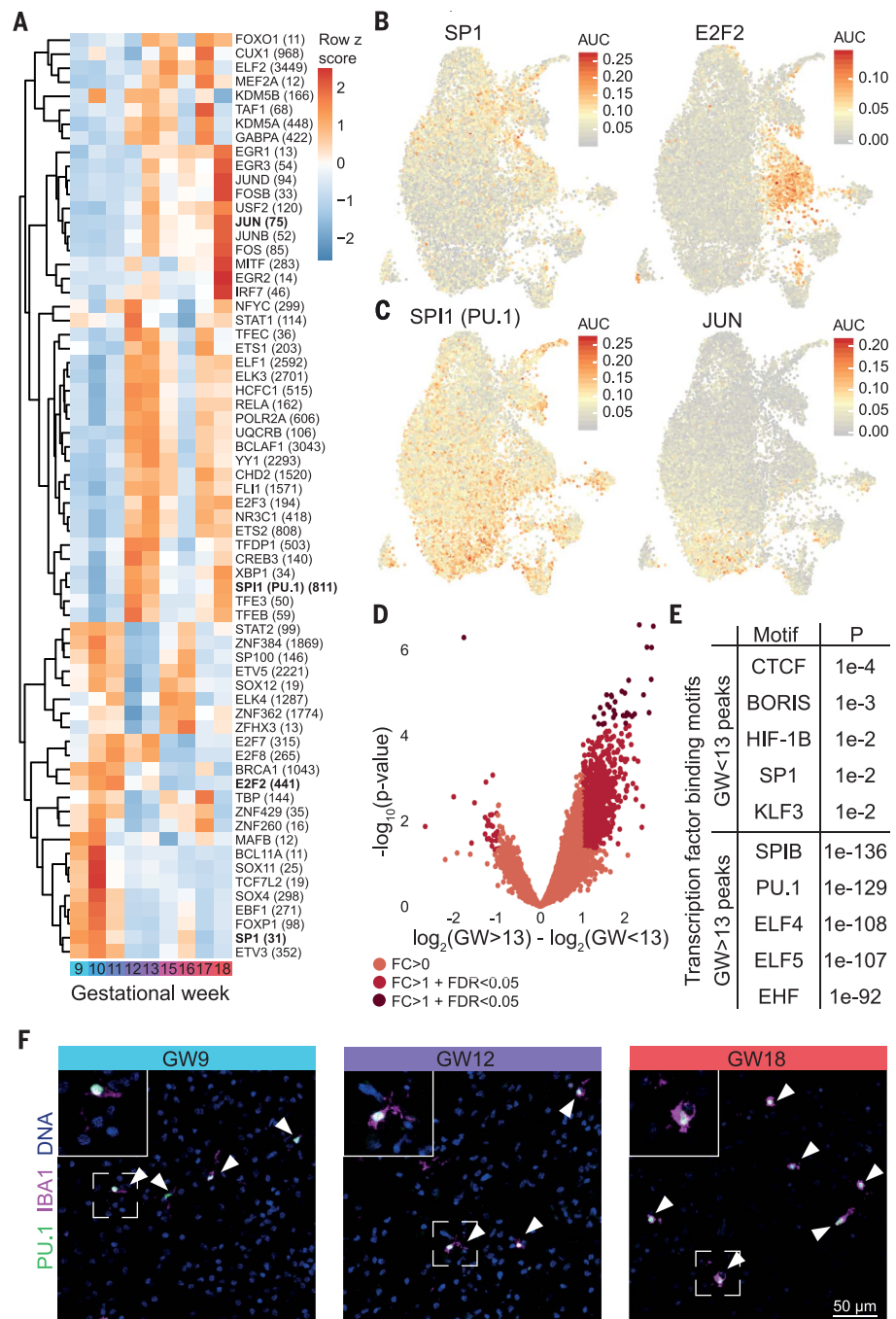


**Fig. 5. Transition of gene regulatory networks and chromatin landscape in microglia during development.** (A) Heatmap with unsupervised clustering of gene regulatory network activity in GW9 to -18 microglia visualized as row z-scores of mean AUC values per GW (20 fetal samples;  $n = 1$  to 4 per GW). (B and C) UMAPs of gene regulatory network activity visualized as AUC values. (D) Volcano plot of differential ATAC peaks between GW>13 and GW<13 microglia (table S8) ( $n = 4$  in each group). (E) TF motif enrichment of sequences underlying differential ATAC peaks. (F) PU.1 and IBA1 coexpression in fetal CNS tissue. White arrowheads indicate colocalization. Insets depict 2 $\times$  magnifications of the indicated areas. FC, fold change; FDR, false discovery rate.

microglia support myelination, neurogenesis (37), and oligodendrogenesis (38). Human microglia may play similar roles, as the gestational period GW9 to -18 coincides with oligodendrocyte (39) and neuronal (40) de-

velopment. These human fetal phagocytic microglia express genes detected in DAM/MGnD microglia that are observed in neurodegenerative mouse models (19–21). The similarities between developmental human microglia

subtypes and DAM/MGnD microglia in mice suggest that developmental transcriptional programs are reactivated in neurodegenerative diseases (*12, 13*) in which microglia are increasingly implicated.

At later GWs, the frequency of IEG-expressing microglia increases. Expression of IEGs in microglia was previously attributed to ex vivo activation (*6, 12*). However, we detected cJUN in fetal CNS tissue prior to microglia isolation, indicating that IEGs were not (exclusively) induced by the isolation procedure or the collection and experimental methods used here. IEG expression might reflect a necessary responsiveness of microglia to local environmental cues of the developing CNS.

In all investigated GWs, small microglia clusters were present (clusters 11 to 16) for which we could not assign specific functional properties because of a low number of cluster-enriched genes. In situ validation of these minor clusters was further hampered by the limited number of cells in these respective clusters and by the small size of early fetal brain tissues.

With increasing GWs, human microglia acquire a more homeostatic phenotype, reflected by an increasing overlap between genes expressed in fetal (especially beyond GW13) and juvenile and adult human microglia. This overlap was likely underestimated, because juvenile and adult human microglia were analyzed by bulk sequencing and may have included less abundantly expressed genes not detected in single-cell sequencing. Moreover, expression of microglia sensome genes (*1*), encoding receptors important in environmental sensing, increased at later gestational ages, pointing to the emergence of immune-sensing microglia during early fetal development. The detected increase in chromatin accessibility and associated gene regulatory networks in fetal microglia from older GWs allows for the activation of more complex gene programs that are required for the immune sensing, synaptic pruning, phagocytic, and tissue-supportive functions of microglia.

The emergence of immune-sensing microglia is highly relevant in view of environmental

perturbations during pregnancy that disturb mouse microglia development (*4, 5*) and impair CNS functions in adult mice (*41*). Perturbed microglial development has been linked to human neurodevelopmental and psychiatric disorders (*8, 9*). A higher risk for the development of autism is associated with feverish infections, particularly in the second trimester (*42, 43*). Because microglia express receptors involved in environmental sensing at this gestational period, they may contribute to fetal CNS sensitivity to the environment during early pregnancy.

Together, our findings demonstrate that microglia are highly heterogeneous during early human fetal development and mature by mid-gestation. This explains the vulnerability of the developing human CNS to environmental perturbations at this developmental period during pregnancy, with potentially long-lasting consequences.

#### REFERENCES AND NOTES

- S. E. Hickman et al., *Nat. Neurosci.* **16**, 1896–1905 (2013).
- P. Füger et al., *Nat. Neurosci.* **20**, 1371–1376 (2017).
- T. L. Tay et al., *Nat. Neurosci.* **20**, 793–803 (2017).
- M. S. Thion et al., *Cell* **172**, 500–516.e16 (2018).
- O. Matcovitch-Natan et al., *Science* **353**, aad8670 (2016).
- P. Ayata et al., *Nat. Neurosci.* **21**, 1049–1060 (2018).
- A. C. Wendeln et al., *Nature* **556**, 332–338 (2018).
- T. L. Tay et al., *Front. Mol. Neurosci.* **10**, 421 (2018).
- M. Prinz, J. Priller, *Nat. Rev. Neurosci.* **15**, 300–312 (2014).
- G. Hoeffel et al., *Immunity* **42**, 665–678 (2015).
- T. Masuda et al., *Nature* **566**, 388–392 (2019).
- Q. Li et al., *Neuron* **101**, 207–223.e10 (2019).
- T. R. Hammond et al., *Immunity* **50**, 253–271.e6 (2019).
- D. A. Menassa, D. Gomez-Nicola, *Front. Immunol.* **9**, 1014 (2018).
- A. Monier et al., *J. Neuropathol. Exp. Neurol.* **66**, 372–382 (2007).
- A. Monier, P. Evrard, P. Gressens, C. Verney, *J. Comp. Neural.* **499**, 565–582 (2006).
- B. B. Lake et al., *Nat. Biotechnol.* **36**, 70–80 (2018).
- S. Zhong et al., *Nature* **555**, 524–528 (2018).
- H. Keren-Shaul et al., *Cell* **169**, 1276–1290.e17 (2017).
- S. Krasemann et al., *Immunity* **47**, 566–581.e9 (2017).
- I. R. Holtzman et al., *Acta Neuropathol. Commun.* **3**, 31 (2015).
- M. Borggrewe et al., *Glia* **66**, 2645–2658 (2018).
- X. Qiu et al., *Nat. Methods* **14**, 979–982 (2017).
- R. Parakalan et al., *BMC Neurosci.* **13**, 64 (2012).
- S. Ghosh, E. Castillo, E. S. Frias, R. A. Swanson, *Glia* **66**, 1200–1212 (2018).
- D. Gosselin et al., *Science* **356**, eaal3222 (2017).
- T. F. Galatro et al., *Nat. Neurosci.* **20**, 1162–1171 (2017).
- S. Aibar et al., *Nat. Methods* **14**, 1083–1086 (2017).
- M. Marin, A. Karis, P. Visser, F. Grosfeld, S. Philipsen, *Cell* **89**, 619–628 (1997).
- A. M. Smith et al., *Glia* **61**, 929–942 (2013).
- K. Kierdorf et al., *Nat. Neurosci.* **16**, 273–280 (2013).
- S. Heinz et al., *Mol. Cell* **38**, 576–589 (2010).
- P. Réu et al., *Cell Rep.* **20**, 779–784 (2017).
- T. Masuda, R. Sankowski, O. Staszewski, M. Prinz, *Cell Rep.* **30**, 1271–1281 (2020).
- M. van der Poel et al., *Nat. Commun.* **10**, 1139 (2019).
- A. Moussaieff et al., *Cell Metab.* **21**, 392–402 (2015).
- A. Włodarczyk et al., *EMBO J.* **36**, 3292–3308 (2017).
- N. Hagemeyer et al., *Acta Neuropathol.* **134**, 441–458 (2017).
- I. Jakovcevski, R. Filipovic, Z. Mo, S. Rakic, N. Zecevic, *Front. Neuroanat.* **3**, 5 (2009).
- I. Kostović, I. Ž. Išasegi, Ž. Krnski, *J. Anat.* **235**, 481–506 (2019).
- D. Mattei et al., *Transl. Psychiatry* **7**, e1120 (2017).
- M. Hornig et al., *Mol. Psychiatry* **23**, 759–766 (2018).
- L. A. Croen et al., *Autism Res.* **12**, 1551–1561 (2019).
- L. Kracht et al., Molecular Neurobiology/Human fetal microglia acquire homeostatic immune-sensing properties early in development, Version v1.1, Zenodo (2020); <https://doi.org/10.5281/zenodo.3835875>.

#### ACKNOWLEDGMENTS

We thank Stichting Stimezo Groningen and Gynaikon Clinic Rotterdam for providing fetal tissue samples. We thank M. Nievene for assistance with sample collections, A. Alsema and M. Meijer for assistance in imaging and data analysis, and the UMCG Central Flow Cytometry Unit for aiding in cell sorting. We thank P. van der Vlies, D. Brandenburg, N. Festen, and W. Uniken Venema for assistance in the implementation of the modified Smart-seq2 protocol, D. Spijkers and K. Hoekstra-Wakker for sequencing-related advice, and D. Smith for scientific editing. **Funding:** L.K. is funded by a fellowship from the Graduate School of Medical Sciences, University of Groningen. M.B. and S.M.K. are supported by the Dutch MS Research Foundation (13-833, 16-947). S.E. holds a scholarship from the Junior Scientific Masterclass, University of Groningen. J.R.P. received a Mandema fellowship, University of Groningen. The Zabawas Foundation (Den Haag, The Netherlands) is thanked for financial support of sequencing.

**Author contributions:** B.J.L.E., L.K., M.B., and S.M.K. contributed to conceptualization. L.K., M.B., N.B., and S.E. designed and performed the experiments. L.K. and M.B. analyzed and visualized the data. B.J.L.E., J.D.L., and S.M.K. acquired funding. B.J.L.E., J.R.P., S.A.S., and S.M.K. contributed to supervision. L.K., M.B., S.E., and S.M.C.d.S.L. collected and isolated tissue samples. M.B., L.K., and B.J.L.E. wrote the manuscript. All authors revised and edited the manuscript.

**Competing interests:** The authors have no competing interests to disclose. **Data and materials availability:** All next-generation sequencing data can be viewed at NCBI GEO under accession number GSE141862. Code used for data analysis is deposited at Zenodo (44).

#### SUPPLEMENTARY MATERIALS

[science.sciencemag.org/content/369/5603/530/suppl/DC1](https://science.sciencemag.org/content/369/5603/530/suppl/DC1)  
Materials and Methods  
Figs. S1 to S5  
Tables S1 to S10  
References (45–57)  
MDAR Reproducibility Checklist

[View/request a protocol for this paper from Bio-Protocol.](https://www.bio-protocol.org/View/Request_a_protocol_for_this_paper_from_Bio-Protocol.html)

16 December 2019; accepted 5 June 2020  
10.1126/science.aba5906

## Human fetal microglia acquire homeostatic immune-sensing properties early in development

L. Kracht, M. Borggrewe, S. Eskandar, N. Brouwer, S. M. Chuva de Sousa Lopes, J. D. Laman, S. A. Scherjon, J. R. Prins, S. M. Kooistra, and B. J. L. Eggen

Science 369 (6503), . DOI: 10.1126/science.aba5906

### The development of microglia

Microglia are the brain's immune cells, and they play important roles in health and neurodegenerative disease. Kracht *et al.* performed single-cell analysis of human microglial gene expression and chromatin accessibility and compared the results with those of other studies of human and mice microglial development. By using *in situ* validation, these data identify fetal microglial subsets that appear to be distinct from adult human microglia, suggesting functional differences between the developing and mature brain.

Science, this issue p. 530

### View the article online

<https://www.science.org/doi/10.1126/science.aba5906>

### Permissions

<https://www.science.org/help/reprints-and-permissions>